Molecular characterization of the craniosynostosis-associated interleukin-11 receptor variants p.T306_S308dup and p.E364_V368del

Birte Kespohl[1], Anna-Lena Hegele[1], Stefan Düsterhöft[2], Hans Bakker[3] (iD), Falk F. R. Buettner[3], Roland Hartig[4], Juliane Lokau[1,3] and Christoph Garbers[3] (iD)

1 Department of Pathology, Medical Faculty, Otto-von-Guericke-University Magdeburg, Germany
2 Institute of Molecular Pharmacology, RWTH Aachen University, Germany
3 Institute of Clinical Biochemistry, Hannover Medical School, Germany
4 Institute for Molecular and Clinical Immunology and Service Unit Multiparametric Bioimaging and Cytometry, Medical Faculty, University of Magdeburg, Germany

Interleukin-11 (IL-11) is a member of the IL-6 family of cytokines and is an important factor for bone homeostasis. IL-11 binds to and signals via the membrane-bound IL-11 receptor (IL-11R, classic signaling) or soluble forms of the IL-11R (sIL-11R, trans-signaling). Mutations in the *IL11RA* gene, which encodes the IL-11R, are associated with craniosynostosis, a human condition in which one or several of the sutures close prematurely, resulting in malformation of the skull. The biological mechanisms of how mutations within the IL-11R are linked to craniosynostosis are mostly unexplored. In this study, we analyze two variants of the IL-11R described in craniosynostosis patients: p.T306_S308dup, which results in a duplication of three amino-acid residues within the membrane-proximal fibronectin type III domain, and p.E364_V368del, which results in a deletion of five amino-acid residues in the so-called stalk region adjacent to the plasma membrane. The stalk region connects the three extracellular domains to the transmembrane and intracellular region of the IL-11R and contains cleavage sites for different proteases that generate sIL-11R variants. Using a combination of bioinformatics and different biochemical, molecular, and cell biology methods, we show that the IL-11R-T306_S308dup variant does not mature correctly, is intracellularly retained, and does not reach the cell surface. In contrast, the IL-11R-E364_V368del variant is fully biologically active and processed normally by proteases, thus allowing classic and trans-signaling of IL-11. Our results provide evidence that mutations within the *IL11RA* gene may not be causative for craniosynostosis and suggest that other regulatory mechanism(s) are involved but remain to be identified.

Introduction

Interleukin-11 (IL-11) is a member of the IL-6 cytokine family [1]. Originally identified as an anti-inflammatory cytokine and approved by the FDA to treat thrombocytopenia in patients undergoing chemotherapy, recent studies have uncovered a plethora of additional functions, especially in developmental

processes, inflammatory diseases and certain types of tumors. These are located e.g. in the stomach [2,3], the colon [4], the breast [5] and the endometrium [6]. Several studies show that blockade of IL-11 signaling offers a therapeutic opportunity for these tumors [4,6].

IL-11 activates its target cells via binding to the membrane-bound IL-11 receptor (IL-11R), whose expression pattern determines which cells can be activated by IL-11. The IL-11R is a type I transmembrane protein that consists of an Ig-like domain (also termed D1 domain), followed by two fibronectin type III domains (the D2 and D3 domains), which contain the cytokine-binding module and are thus required for ligand binding. The D3 domain contains the typical WSXWS motif found in all class I cytokine receptors [7]. The three extracellular domains are followed by a stalk region, which connects them to a transmembrane helix and an intracellular region [8]. The intracellular region is not required for the activation of signaling cascades but contains motifs required for IL-11R sorting in polarized cells [9]. Formation of the IL-11/IL-11R complex leads to the recruitment and homodimerization of two molecules of the signal-transducing β-receptor gp130, which then activates intracellular signaling cascades, including the Jak/STAT, PI3K and ERK pathways [10,11].

We have previously shown that also soluble variants of the IL-11R (sIL-11R) exist [12–15]. IL-11 binds to the sIL-11R with similar affinity as to the membrane-bound IL-11R, and the resulting IL-11/sIL-11R complex can agonistically activate cells via gp130 homodimerization, a mode of action that has been termed IL-11 trans-signaling [14]. Olamkicept (sgp130Fc), which is currently in clinical development and has been successfully used to treat patients with inflammatory bowel disease in an open-label, prospective phase 2a trial [16] and a randomized, double-blind, placebo-controlled phase 2 trial [17], is also an effective inhibitor of IL-11 trans-signaling [14,18]. We have shown previously that sIL-11R is generated by proteolytic cleavage of the membrane-bound IL-11R and that this can be performed by different proteases, including the metalloprotease ADAM10 [14,19], the neutrophil-derived serine proteases neutrophil elastase and proteinase 3 [14] and the rhomboid-like protease RHBDL2 [12]. sIL-11R can be detected in the serum of healthy volunteers [14] and is part of the human plasma proteome [20]. However, a functional role has not been established yet.

Besides its pro-inflammatory role, IL-11 has important functions in developmental processes. It is required for female fertility [21–23] and bone homeostasis (reviewed in [24]). A single nucleotide polymorphism (SNP) within IL-11 causes instability of the protein [25] and is linked to reduced height in human adults [26,27]. Furthermore, several mutations within the *IL11RA* gene, which encodes the IL-11R, have been reported in patients with craniosynostosis. Craniosynostosis is a human condition in which one or several of the sutures which line the head bones close prematurely, resulting in malformation of the skull and several accompanying symptoms [28–32]. The *IL11RA* is not the only gene in which coding variants have been linked to craniosynostosis. Previous studies reported variants in *MSX2*, *TWIST1*, *RAB23* and especially in the fibroblast growth factor-receptor encoding genes *FGFR1*, *FGFR2* and *FGFR3* in patients with craniosynostosis [32–34].

IL-11 supports differentiation of osteoblasts and osteoclasts and is important for osteoblast function. Mutations which cause craniosynostosis are known to either increase the proliferation of osteoblast precursor cells or to induce their premature differentiation into osteoblasts [29]. Previous studies reported a reduction in bone formation and resorption in $Il11ra^{-/-}$ mice *in vivo* and impaired osteoclast differentiation *in vitro* [35], suggesting that a defect in bone resorption as the underlying cause for premature closure of the sutures in human patients. However, the definite functional role of IL-11 in skull development and why lack of IL-11 signaling results in craniosynostosis is not entirely clear.

Biological studies exploring the underlying (patho) mechanisms are lacking for most of the IL-11R variants. Our previous work has shown that the four IL-11R mutations P200T, P221R, R296W, and W307R result in no functional IL-11R at the cell surface [36,37]. After translation, the IL-11R is transported through the endoplasmic reticulum (ER) and the Golgi apparatus before being inserted into the plasma membrane. The amino-acid sequence of the IL-11R contains two sequons for *N*-linked glycosylation at the two asparagine residues N127 and N194 [38]. *N*-glycosylation is initiated in the ER, and the sugar chains are then further processed in the Golgi. Therefore, the fully matured IL-11R at the plasma membrane has a higher molecular weight compared to intermediates still located in intracellular organelles [36,38]. Additionally, the ER has an important role in terms of quality control, as it retains not correctly folded proteins and prevents their onward transportation to the Golgi. For the IL-11R-R296W variant, we have shown that it is retained within the ER and not transported further to the Golgi [36]. Furthermore, IL-11R-R296W and the three other IL-11R variants lack the fully matured IL-11R band when analyzed by western blot, confirming incomplete maturation of the

IL-11R. In contrast, different IL-11R variants annotated in the genome aggregation database (gnomAD, [39]) differ in their amount at the cell surface, but show in principle normal biological function [40].

In this study, we analyze a duplication (c.916_924dup/p.T306_S308dup) and a deletion variant (c.1090_1104delGAGCAGGTAGCTGTG/p.E364_V368del) variant of the IL-11R. We find that the duplication affects the WSXWS motif within the D3 domain, prevents maturation and transport to the cell surface and results in a complete loss-of-function. In contrast, the deletion of five amino-acid residues in the stalk region is tolerated and the IL-11R variant is fully functional.

Results

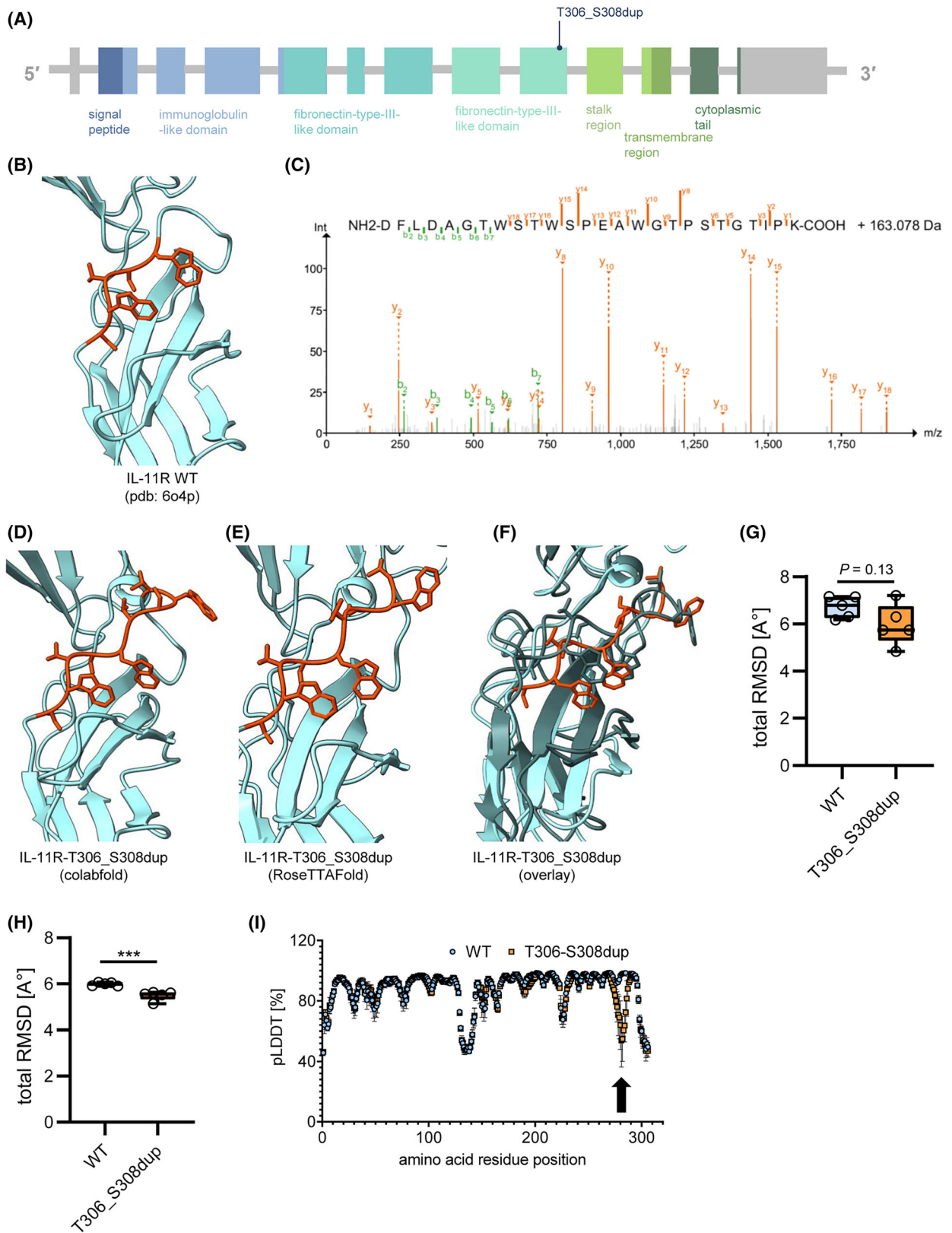### The mutation p.T306_S308dup affects the WSXWS motif within the D3 domain of the IL-11R

The duplication p.T306_S308dup is located within exon 9 of the *IL11RA* gene, which encodes part of the membrane-proximal fibronectin type III domain (termed D3) of the IL-11R (Fig. 1A). Intriguingly, the duplication occurs within the so-called WSXWS motif, an important feature shared upon all class I cytokine receptors [41–43]. It represents a classical site for *C*-mannosylation, a post-translational modification that was shown to be vital for ER exit [44,45]. For the IL-11R, this motif is formed by W304, S305, T306, W307 and S308 (Fig. 1B). Because no data are available whether the IL-11R is indeed *C*-mannosylated, we subsequently reanalyzed raw public proteomic data for modified peptides of the IL-11R. The IL-11R-derived tryptic peptide containing the potential site for *C*-mannosylation with an additional mass of 163 Da was identified by Fragpipe in open search mode (Fig. 1C). Manual evaluation of y- and b-ions led to an unambiguous identification of the respective peptide. The mass difference of 163 Da can be explained by addition of one hexose in combination with a selection of the second isotope peak for fragmentation. We confirmed the latter by a view at the MS spectrum at the retention time of the identified MS2 spectrum. Unequivocal proof that the hexose was localized on the first tryptophan could not be obtained as the b- and y-ions did not cover this amino acid residue.

Due to the duplication of the three amino-acid residues T306_S308, the IL-11R variant has an extension of the usual motif with an additional WS (WSXWSXWS), which should also represent a motif for *C*-mannosylation. Because no structure for this IL-11R variant is available, we used COLABFOLD [46] and

ROSETTAFOLD [47] to obtain five structural models of IL-11R-T306_S308dup by each algorithm. The best structures of both algorithms showed alterations in the loop that contains the WSXWS motif (Fig. 1D,E). Importantly, both structural models were in pretty good agreement with each other with a root mean square deviation (RMSD) of 5.095 Å over all atom pairs (Fig. 1F). In addition, we tried to determine whether we could use the structural models of IL-11R-T306_S308dup to predict *in silico* whether the duplication of three amino-acid residues has an impact on the overall backbone structure of the IL-11R. For this, we next used COLABFOLD to generate models of the IL-11R-WT structure and compared these and the COLABFOLD-generated models of IL-11R-T306_S308dup to the crystal structure of the IL-11R. We observed a reduced overall RMSD of the whole structures of IL-11R-T306_S308dup compared to IL-11R-WT ($P = 0.13$, Fig. 1G), indicating that the duplication may indeed cause alterations of the IL-11R structure that are detectable using this method. We then performed the same analysis with the structural models generated by ROSETTAFOLD. The overall RMSD was significantly lower for IL-11R-T306_S308dup compared to IL-11R-WT ($P < 0.001$, Fig. 1H). We also observed a sharp drop of the per-residue confidence score (pLDDT) at the site of the duplication, which was not seen for the IL-11R-WT, likely due to steric hindrance by the extra residues (Fig. 1I). Altogether, these results suggest that the duplication affects the backbone of the IL-11R structure and could possibly compromise its biological function.

The mutation p.E364_V368del is located in the stalk region of the IL-11R

The deletion p.E364_V368del is located within the stalk region of the IL-11R in close proximity to the transmembrane region (Fig. 2A). The stalk region connects the three extracellular domains to the plasma membrane and has to be of a certain length in order to allow signaling [48]. Furthermore, several cleavage sites used by different proteases to generate soluble forms of the IL-11R, thereby initiating trans-signaling, exist within the stalk region in close proximity to the here analyzed deletion [12,14]. We have previously shown that cleavage by the metalloprotease ADAM10 requires Arg-355 (Fig. 2B and [14]). It is possible that the deletion of the five amino-acid residues in the variant IL-11R-E364_V368del, therefore, affects ADAM10-mediated cleavage. However, this appears rather unlikely, as a deletion variant encompassing 10 amino-acid residues (V363_L372) was still efficiently

(A)

T306_S308dup

signal peptide

immunoglobulin -like domain

fibronectin-type-III- like domain

fibronectin-type-III- like domain

stalk region

transmembrane region

cytoplasmic tail

(B)

IL-11R WT
(pdb: 6o4p)

(C)

NH2-D F L D A G T W S T W S P E A W G T P S T G T I P K-COOH + 163.078 Da

(D)

IL-11R-T306_S308dup
(colabfold)

(E)

IL-11R-T306_S308dup
(RoseTTAFold)

(F)

IL-11R-T306_S308dup
(overlay)

(G)

(H)

(I)

Fig. 1. The mutation p.T306_S308dup affects the WSXWS motif within the D3 domain of the IL-11R. (A) Schematic representation of the exons encoding the IL-11R protein. The individual domains of the IL-11R are given in the same color code as the exons. The T306_S308dup mutation within the D3 domain is indicated. (B) Section of the crystal structure of the IL-11R (pdb: 6O4P [61]) containing parts of the D2 and D3 domains. The amino acid residues which form the WSXWS motif within the D3 domain are highlighted in red. (C) MS2 spectrum of a 2+ ion of 1486.194 Da, which has a delta mass of 163.078 compared to the calculated monoisotopic mass of the peptide (2807.308 Da) derived from sample 20200724_cell_18 spectrum number 48328 of reanalyzed proteomics data from a brain cancer cell line [50]. (D, E) Sections of models of IL-11R-T306_S308dup generated by COLABFOLD [46] and ROSETTAFOLD [47] containing parts of the D2 and D3 domains. The amino acid residues which form the extended WSXWS motif within the D3 domain are highlighted in red. (F) Overlay of the structures shown in panels D and E. The structure generated by COLABFOLD is shown in dark petrol, whereas the structure generated by ROSETTAFOLD is shown in the same colors as in panel D. Visualization of the structures in panels B to F was done with CHIMERAX. (G) Structural models of IL-11R-WT were generated by COLABFOLD. They were compared to the crystal structure of the IL-11R (pdb: 6O4P) in terms of total RMSD (light blue bars). Similarly, the COLABFOLD-generated models of IL-11R-T306_S308dup were compared to the crystal structure of the IL-11R (orange bars). Five models were analyzed per condition and shown as box and whiskers plots with all individual data points including the mean $\pm$ SD. Statistical analysis was performed by two-tailed unpaired *t*-tests. (H) The experiment was performed as described for the previous panel, but with the ROSETTAFOLD-generated structural models. Five models were analyzed per condition and shown as box and whiskers plots with all individual data points including the mean $\pm$ SD. Statistical analysis was performed by two-tailed unpaired *t*-tests (***: $P < 0.001$). (I) Plot of the pLDDT scores of the IL-11R-WT and IL-11R-T306_S308dup models generated by COLABFOLD (mean $\pm$ SD, $n = 5$). The drop of the pLLDT score due to the duplication is marked by a black arrow.

cleaved by ADAM10 [14]. Additionally, the rhomboid protease RHBDL2 cleaves the IL-11R at position Ala-370, which is in close proximity to the deletion in this IL-11R variant (Fig. 2B and [12]). Previous work has shown that the aforementioned deletion variant IL-11RΔV363-L372 was resistant toward RHBDL2-mediated cleavage. However, this deletion included the actual cleavage site. In contrast, deletion of 10 amino-acid residues further N-terminal (H353_S362) did not affect proteolysis by RHBDL2 at all [12]. It is therefore tempting to speculate how the deletion will affect proteolysis of this IL-11R variant. Of note, the stalk region is considered flexible and non-structured and is therefore not included in the crystal structure of the IL-11R, preventing a comparison between structural models of IL-11R-E364_V368del and IL-11R-WT. Indeed, a structural model by COLABFOLD showed a very low certainty for the stalk region in contrast to the three extracellular domains (Fig. 2C).

Impaired maturation and lack of cell-surface appearance of IL-11R-T306_S308dup, but not of IL-11R-E364_V368del

We further sought to complement our *in silico* analyses with biochemical data to confirm or refute our results. For this purpose, we generated expression plasmids encoding IL-11R-T306_S308dup and IL-11R-E364_V368del, respectively, fused to an N-terminal Myc-tag. We have used similar constructs in previous studies and therefore know that a small tag at the N-terminus does not affect the biological activity of the IL-11R [12,14,36,40]. We transiently expressed both constructs and IL-11R-WT and IL-11R-R296W, which we have previously shown to be misfolded and thus

inactive, as controls in HEK293 cells and analyzed IL-11R expression via western blot. In line with our previous results [12,36,40], IL-11R-WT was detected as at least three distinct bands, whereas IL-11R-R296W lacked the band with the highest molecular weight (Fig. 3A). We have previously shown that the upper band corresponds to the fully matured IL-11R at the plasma membrane and that IL-11R-R296W, therefore, does not mature properly and is not transported to the cell surface [36,38]. We detected two bands for IL-11R-T306_S308dup and three bands for IL-11R-E364_V368del, suggesting that the latter one matures properly, whereas the duplication has a defect in maturation (Fig. 3A).

We further substantiated this finding by analyzing *N*-linked glycosylation of both IL-11R variants. In a previous study, we have shown that overexpressed IL-11R is *N*-glycosylated at the two asparagine residues N127 and N194 [38]. Whether this holds true *in vivo* is not known. Therefore, we reanalyzed public raw proteomic data for modified peptides of the IL-11R. One identified peptide covered one of the two putative *N*-glycosylation sites (N194) (Fig. 3B). This showed the characteristics of an *N*-glycosylated peptide with a peak pattern of the naked peptide and y-ions with one and two HexNAcs. In addition, the MS2 spectrum contained the typical glycan fragments. However, we could not assign the exact *N*-glycan structure to the observed additional mass of 1866.641 Da. The same peptide has been identified in deaminated form after cleavage of *N*-glycans, indicating its *N*-glycosylation, in proteomic data of gastric cancer samples [49]. The other potentially *N*-glycosylated peptide was not found in these experiments. We also did not find this N127 containing peptide in *N*-glycosylated form in the

(A)

(B)

(C)
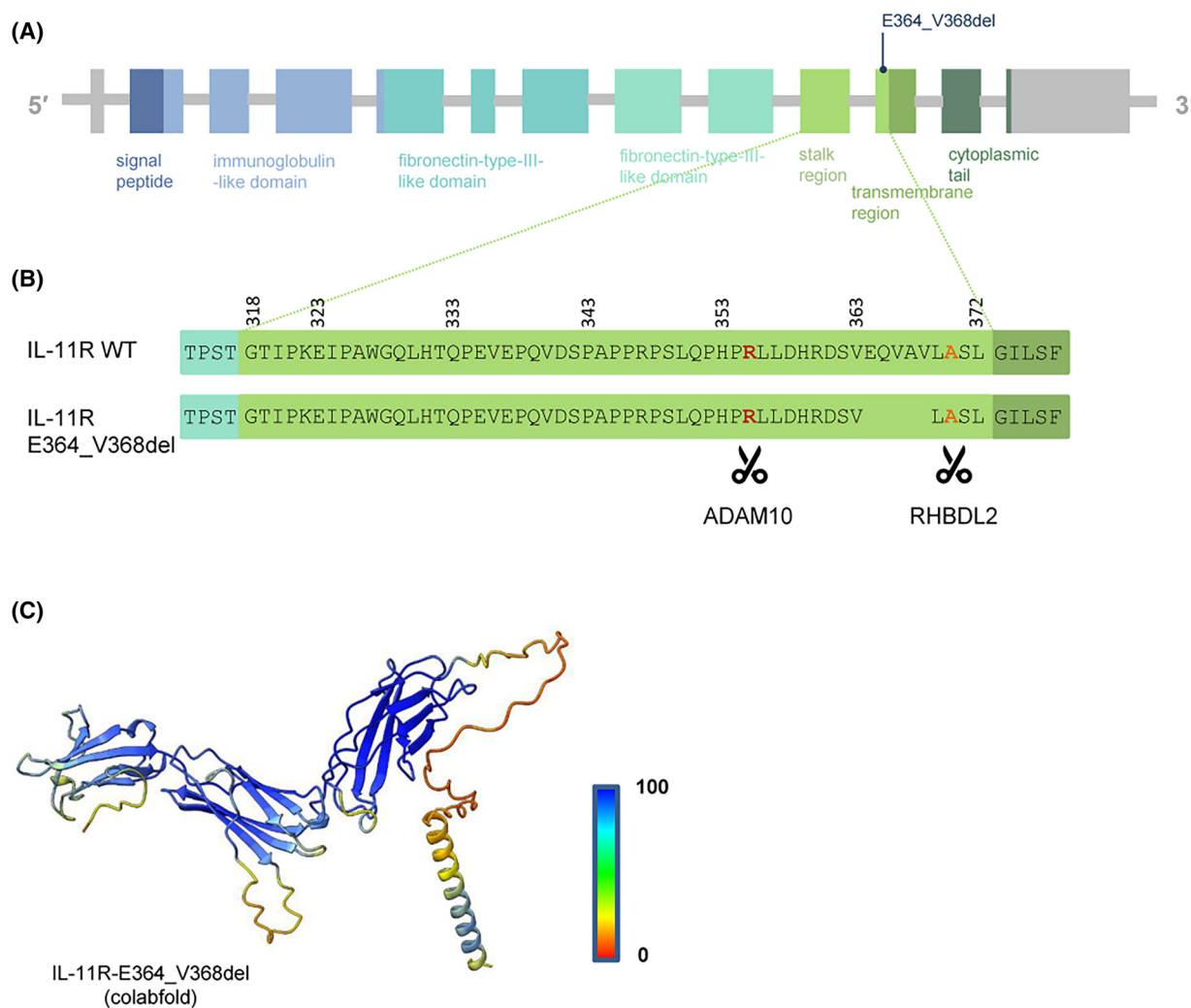
Fig. 2. The mutation p.E364_V368del is located in the stalk region of the IL-11R. (A) Schematic representation of the exons encoding the IL-11R protein. The individual domains of the IL-11R are given in the same color code as the exons. The E364_V368del mutation within the stalk region is indicated. (B) Close-up of the stalk region showing the amino-acid residues from Gly (G)-318 to Leu (L)-372 according to [48]. The sequence of IL-11R-WT and of IL-11R-E364_V368del are shown. Arg (R)-355, which is important for proteolytic cleavage by ADAM10 [14], is highlighted in bold red. Ala (A)-370, which is important for proteolytic cleavage by RHBDL2 [12], is highlighted in bold orange. (C) COLABFOLD-generated model of the IL-11R-E364_V368del variant. The highest ranked model is depicted in cartoon representation colored according to the pLDDT (predicted local distance difference test) score in [%].

reanalysis of the brain cancer cell line data of Zhang *et al*. [50]. They, however, identified this peptide in a non-glycosylated form in their analysis.

IL-11R-T306_S308dup appeared as two distinct bands upon western blotting and treatment with PNGaseF led to one sharp band with reduced molecular weight. This observation suggests that the two variants of IL-11R-T306_S308dup are caused by different types or degrees of *N*-glycosylation. In contrast, IL-11R-E364_V368del displayed as one major and two heavier, but less intensive variants on the blot and treatment with PNGase F similarly reduced the

molecular weight of all these variants but did not result in a single molecular weight form. Therefore, we assume that all size-variants of IL-11R-E364_V368del contain a PNGaseF-sensitive *N*-glycosylation. As there are still three size-variants upon the digestion, there must be different degrees of a PNGaseF-insensitive posttranslational modification, which could be *O*- or *C*-glycans. These findings would fit to our model that glycosylation of IL-11R-E364_V368del properly matured while the protein passed through the Golgi, similar to IL-11R-WT, while IL-11R-T306_S308dup was retained within the cell (Fig. 3C). In line

with that, we could detect via flow cytometry that the IL-11R-E364_V368del and the IL-11R WT were present at the plasma membrane in stably transduced Ba/F3-gp130 cell lines (Fig. 3D). In contrast, both IL-11R-R296W and IL-11R-T306_S308dup were not detectable at the cell surface (Fig. 3D). Finally, we used confocal microscopy to analyze cell-surface localization of the four IL-11R variants in transiently transfected HeLa cells. We first stained non-permeabilized cells and could clearly detect IL-11R-WT and IL-11R-E364_V368del at the cell surface where they co-localized with the plasma membrane marker WGA (Fig. 3E). IL-11R-T306_S308dup could not be detected at the cell surface, which is in line with our previous results arguing for improper maturation and subsequently intracellular retention. Of note, when we permeabilized the cells to allow staining of IL-11R species inside of the cell, all variants were visible, confirming that the difference is really due to intracellular transport and not simply a lack of expression of IL-11R-T306_S308dup (Fig. 3E).

Biological activity of Ba/F3-gp130-IL-11R-T306_S308dup and Ba/F3-gp130-IL-11R-E364_V368del

Having analyzed the expression and maturation of the two IL-11R variants, we next wanted to determine their biological activity. For this purpose, we used stably transduced Ba/F3-gp130 cell lines. Ba/F3 cells are murine pre-B cells that proliferate in the presence of IL-3 and undergo apoptosis otherwise. Stable expression of gp130 and IL-11R makes them susceptible to stimulation by IL-11 and Ba/F3 cells are therefore a versatile tool to investigate the biological function of IL-11R variants. We first serum-starved Ba/F3-gp130-IL-11R-WT, Ba/F3-gp130-IL-11R-R296W, Ba/F3-gp130-IL-11R-T306_S308dup and Ba/F3-gp130-IL-11R-E364_V368del and stimulated them with either 10 ng·mL^{-1} Hyper-IL-6, 10 ng·mL^{-1} IL-11 for 15 min or left them untreated. Hyper-IL-6 is a fusion protein of IL-6 and the sIL-6R that directly activates a gp130 homodimer without the need for a functional alpha-receptor and serves as the positive control. We observed an increase in phosphorylation of the transcription factor STAT3 in all four cell lines when stimulated with Hyper-IL-6 compared to unstimulated cells (Fig. 4A). In contrast, only Ba/F3-gp130-IL-11R-WT and Ba/F3-gp130-IL-11R-E364_V368del cells responded to IL-11 stimulation (Fig. 4A), confirming our previous experiments that demonstrated absence of IL-11R at the cell surface for Ba/F3-gp130-IL-11R-R296W and Ba/F3-gp130-IL-11R-T306_S308dup (Fig. 3D and [36]).

Further, full maturation of the IL-11R was only visible for IL-11R-WT and IL-11R-E364_V368del, but not for IL-11R-R296W and IL-11R-T306_S308dup, via western blot (Fig. 4A). Because we did not want to rely on a single time point, we next performed a kinetic experiment over 120 min. As shown in Fig. 4B, the phosphorylation of STAT3 in Ba/F3-gp130-IL-11R-WT cells peaked 30 min after stimulation and declined afterward. In contrast, we observed no pSTAT3 over 120 min in Ba/F3-gp130-IL-11R-T306_S308dup cells, underlining that this cell line is completely unable to be activated by IL-11 and has not just an altered pSTAT3 kinetic that is not detectable 15 min after stimulation (Fig. 4C). Ba/F3-gp130-IL-11R-E364_V368del cells phenocopied Ba/F3-gp130-IL-11R-WT cells, indicating no influence of the deletion on IL-11-mediated signaling (Fig. 4D).

Finally, we analyzed the viability of the different Ba/F3-gp130 cell lines over 48 h. Ba/F3-gp130-IL-11R-WT cells proliferated in a dose-dependent manner when stimulated with increasing amounts (0–100 ng·mL^{-1}) of either Hyper-IL-6 or IL-11 (Fig. 4E). Ba/F3-gp130-IL-11R-R296W and Ba/F3-gp130-IL-11R-T306_S308dup only proliferated in the presence of Hyper-IL-6, but not when stimulated even with high amounts of IL-11 (Fig. 4F,G). In line with our previous results, Ba/F3-gp130-IL-11R-E364_V368del cells responded to both Hyper-IL-6 and IL-11 stimulation (Fig. 4H). Taken together, these results show that IL-11R-E364_V368del is biologically functional, whereas cells expressing Ba/F3-gp130-IL-11R-T306_S308dup are not able to respond to stimulation by IL-11.

Proteolysis of IL-11R-E364_V368del results in trans-signaling of soluble IL-11R-E364_V368del

We have previously shown that proteolytic cleavage of the IL-11R results in the generation of a sIL-11R that, in combination with IL-11, can perform trans-signaling [13,14,51,52]. Proteolysis by ADAM10 is thought to occur at the plasma membrane, and we therefore first analyzed ADAM10-mediated shedding for IL-11R-WT and IL-11R-E364_V368del. For this, we transiently transfected HEK293 cells, stimulated them 48 h after transfection for 60 min with the calcium ionophore ionomycin, and determined sIL-11R in the supernatant. Both IL-11R variants were indeed cleaved, suggesting that the reduced distance between the plasma membrane and the critical amino-acid residue Arg-355 does not significantly alter cleavage by ADAM10 (Fig. 5A). As RHBDL2 is able to cleave IL-11R even within the ER [12], we next analyzed cleavage of both IL-11R-T306_S308dup and IL-11R-E364_V368del by this protease. We co-expressed the two IL-11R variants either
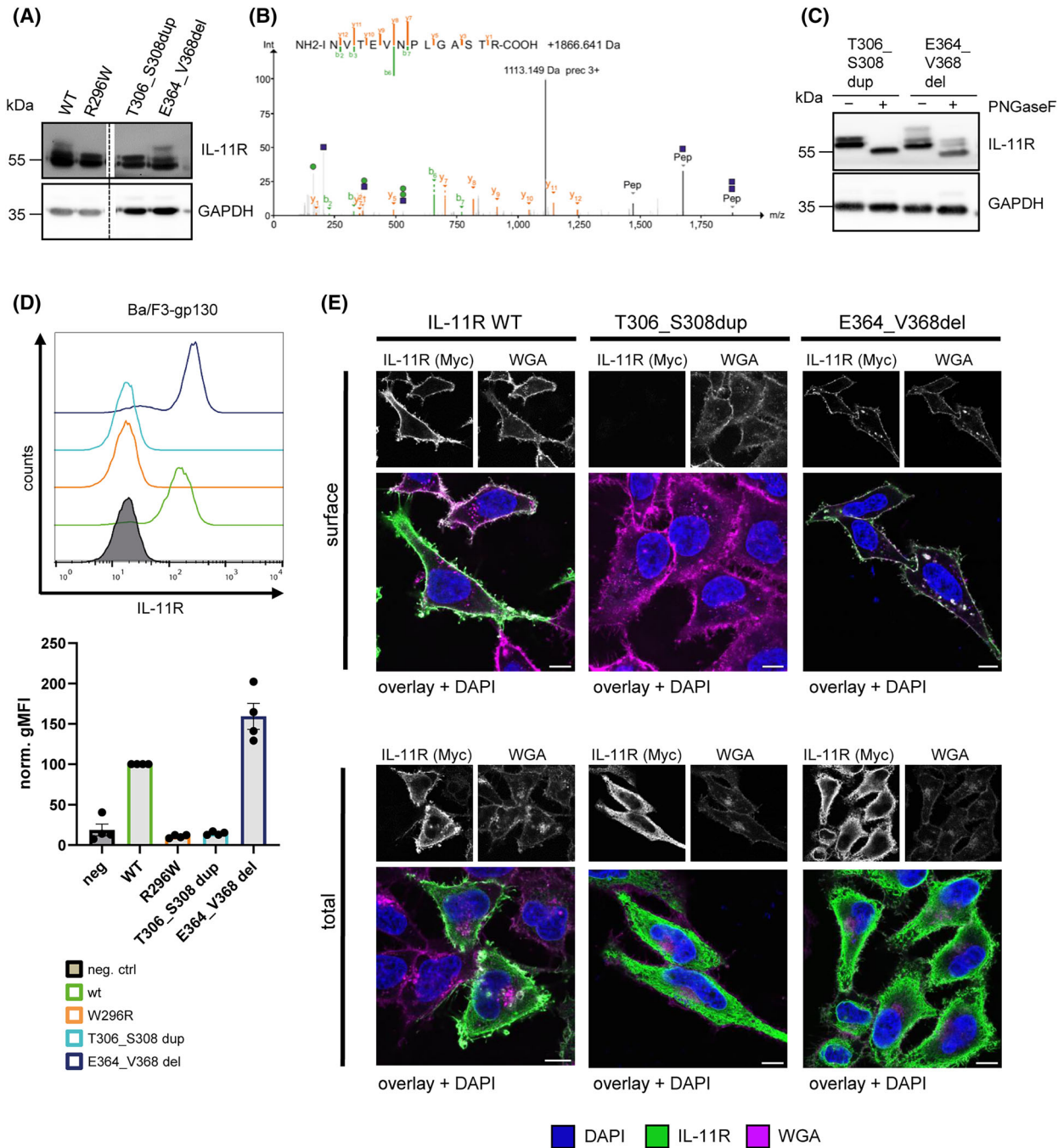
with RHBDL2 or mCherry as control transiently in HEK293 cells and analyzed IL-11R cleavage in the cell lysate and sIL-11R generation in the cell supernatant via western blot. As shown in Fig. 5B, both IL-11R variants were proteolytically processed by RHBDL2, as seen by the occurrence of a band of lower molecular weight in the cell lysate whenever RHBDL2 was present, indicating that the duplication and the deletion do not alter RHDBL2 cleavage *per se*. However, sIL-11R could only

be detected in the supernatant of cells expressing IL-11R-E364_V368del, but not IL-11R-T306_S308dup. This indicates that the cleaved form of IL-11R-T306_S308dup is retained within the cell and not released into the cell culture supernatant, most probably due to misfolding caused by the duplication. Finally, we added IL-11 to supernatants containing RHBDL2-cleaved sIL-11R-WT or sIL-11R-E364_V368del and found that like its wild-type counterpart, sIL-11R-

Fig. 3. Impaired maturation and lack of cell-surface appearance of IL-11R-T306_S308dup, but not of IL-11R-E364_V368del. (A) HEK293 cells were transiently transfected with expression plasmids encoding the indicated IL-11R variants. 48 h later, the cells were harvested, lysed and analyzed by western blotting. GAPDH was detected on the same membrane in order to ensure equal protein loading. Samples unrelated to this manuscript have been spliced out. One of three experiments with similar outcome is shown. (B) MS2 spectrum of a 3+ ion of 1113.149 Da, which has a delta mass of 1866.641 compared to the monoisotopic mass of the peptide (1469.784 Da), from a sample (20200721_cell_18 spectrum 25 355) from a from a brain cancer cell line [50]. Green circle: hexose (162 Da), Blue square: HexNAc (203 Da). (C) Lysates of HEK293 cells transiently transfected with expression plasmids encoding either IL-11R-T306_S308dup or IL-11R-E364_V368del were left untreated or treated with PNGaseF. One of three experiments with similar outcome is shown. (D) Cell surface expression of the different IL-11R variants stably expressed in Ba/F3-gp130 cells were analyzed via flow cytometry. Shown is one of three independent experiments with similar outcome and the quantification of normalized geometric mean fluorescence intensity in all three experiments in panel D (mean ± SD). (E) Immunofluorescence staining of IL-11R-WT, IL-11R-T306_S308dup and IL-11R-E364_V368del in HeLa cells. HeLa cells were seeded on coverslips and transiently transfected with expression plasmids encoding the indicated IL-11R variants. 48 h after transfection, cells were fixed and stained with DAPI, myc antibody, and wheat germ agglutinin (WGA) using a blocking solution with saponin (permeabilized, total staining) or without saponin (non permeabilized, surface staining). Stained slides were visualized on a confocal microscope. Scale bar: 10 μm.

E364_V368del in complex with IL-11 was able to induce IL-11 trans-signaling via phosphorylation of STAT3 (Fig. 5C). In conclusion, our results show that RHBDL2 is able to cleave both IL-11R variants independent of their cellular localization, but that only cleavage of the IL-11R-E364_V368del variant results in the release of a soluble IL-11R in the cell supernatant.

Discussion

Mutations within the *IL11RA* gene have been identified in patients with craniosynostosis [28–32]. For most of these mutations, it is unclear how they affect the receptor and which mechanisms cause the phenotype of the patients. Our previous studies comprising four point mutations (P220T, P221R, R296W and W307R) showed unequivocally that these IL-11R variants do not mature properly, do not reach the cell surface and thus result in a total loss of IL-11 signaling in these patients [36,37]. We have recently additionally analyzed five point mutations annotated in the gnomAD database [39] and found that some of these mutations alter the amount of IL-11R at the cell surface, but that nevertheless all of these variants are biologically active [40]. Based on these two studies, one could assume that IL-11R variants that do not reach the cell surface cause craniosynostosis in humans, whereas other mutants that do not significantly affect IL-11R function are tolerated and do not cause a phenotype with craniosynostosis-like features.

The results of this study do not fully support this simplistic view. The duplication variant IL-11R-T306_S308dup behaves as we have seen for the four point mutations studied previously. IL-11R-T306_S308dup is expressed in different cell lines at levels comparable to IL-11R-WT and other IL-11R variants, but shows a severe maturation defect (Fig. 5D). The band with the highest molecular weight corresponding to the mature IL-11R is absent in western blots, and no IL-11R can be detected at the cell surface, resulting in a complete loss of IL-11 signaling in cells expressing this variant. Digestion with PNGaseF which removes *N*-linked oligosaccharides, led to a single molecular weight variant for IL-11R-T306_S308dup whereas still different size variant could be observed for IL-11R-E364_V368del. Therefore, we hypothesize that IL-11R-T306_S308dup is retained within the cell and does achieve a mature pattern of glycosylation (Fig. 5D). The affected *C*-mannosylation motif is known to be an important ER-exit feature [45]. Recently, Shcherbakova *et al.* [44] demonstrated that *C*-mannosylation supports the stability of proteins in the ER. The duplication within the *C*-mannsylation motif WSXWS motif leads to WSXWSXWS, which itself would also represent a *C*-mannosylation motif. However, whether this simple extension of the sequence translates to a functional *C*-mannsylation motif in IL-11R-T306_S308dup is currently unknown. It is well established that the quality control systems in the ER ensure that only properly folded glycoproteins are allowed to exit and to progress to the Golgi apparatus [53–55]. Therefore, it is safe to assume that the duplication results in at least partial misfolding of the IL-11R and thus intracellular retention of this variant.

Our MS data verify that the endogenous IL-11 receptor is both *C*-mannosylated and *N*-glycosylated. The double band shown in the western blot of IL-11R-T306_S308dup, which converts to a single lower band after digestion of the *N*-glycans (Fig. 3C), suggests that one site is fully occupied and a second site only partially. The MS data indicate that N194 is the site that is probably fully used.
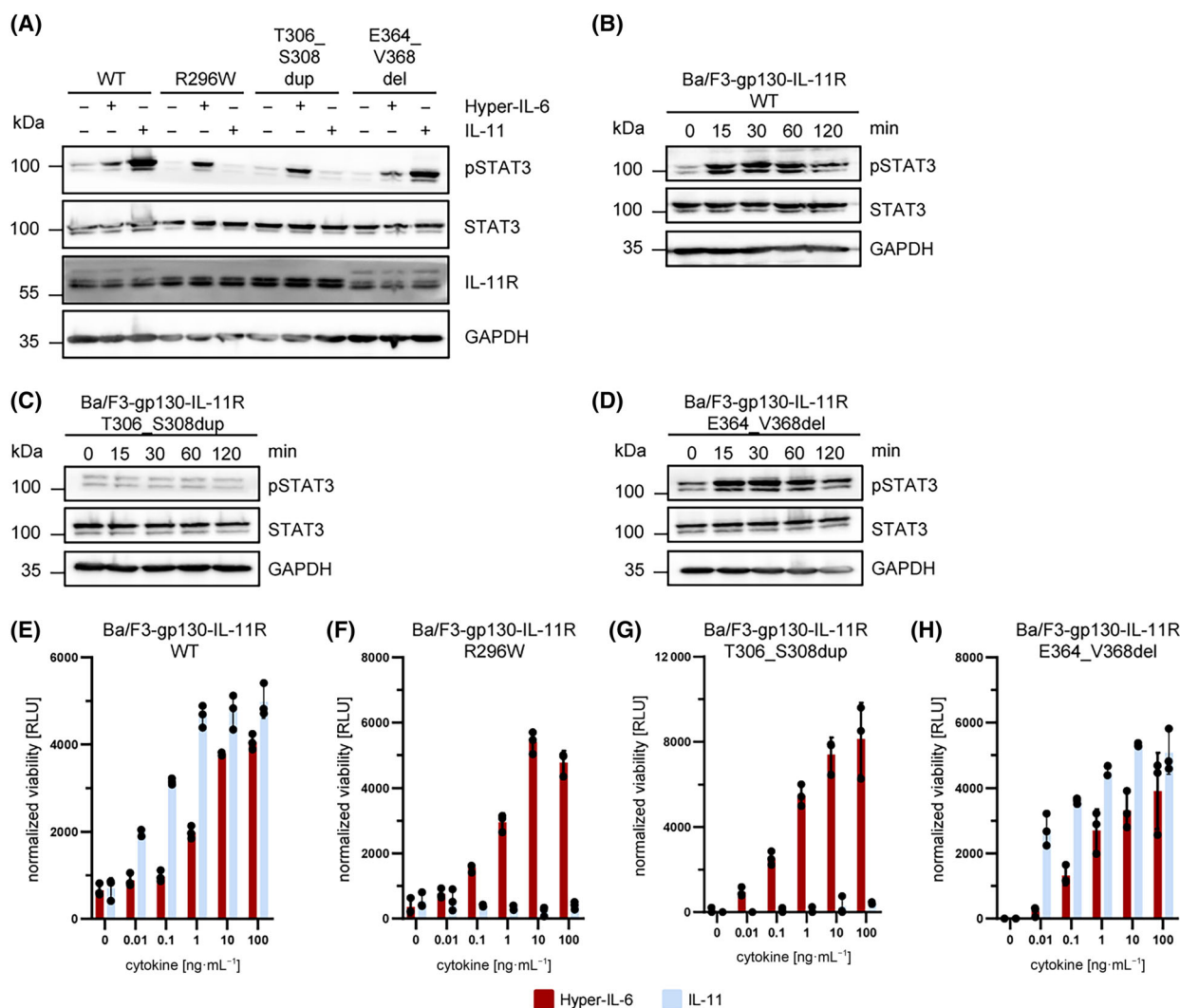
Fig. 4. Biological activity of Ba/F3-gp130-IL-11R-T306_S308dup and Ba/F3-gp130-IL-11R-E364_V368del. (A) Equal amounts of Ba/F3-gp130 cells stably expressing the indicated IL-11R variants were stimulated for 15 min with either 10 ng·mL^{-1} Hyper-IL-6, 10 ng·mL^{-1} IL-11 or left unstimulated. Cells were lysed and phosphorylation of STAT3 and IL-11R expression were determined via western blotting. Total STAT3 levels and GAPDH were visualized to ensure equal protein loading. Shown is one representative western blots of three independent experiments with similar outcome. (B–D) Equal numbers of stably transduced Ba/F3-gp130 cells expressing (B) IL-11R-WT, (C) IL-11R-T306_S308dup and (D) IL-11R-E364_V368del were stimulated for 0–120 min with recombinant IL-11 (10 ng·mL^{-1}). Cells were lysed and phosphorylation of STAT3 was determined via western blotting. Total STAT3 levels and GAPDH were visualized to ensure equal protein loading. All panels show representative western blots of three independent experiments with similar outcome. (E–H) Equal numbers of (E) Ba/F3-gp130-IL-11R-WT, (F) Ba/F3-gp130-IL-11R-R296W, (G) Ba/F3-gp130-IL-11R-T306_S308dup and (H) Ba/F3-gp130-IL-11R-E364_V368del cells were incubated in triplicates with increasing amounts (0–100 ng·mL^{-1}) of either recombinant IL-11 or Hyper-IL-6. After 48 h, cell viability was measured. Shown are the mean ± SD from one representative experiments out of three independent experiments with similar outcome.

In contrast to the duplication variant, the deletion variant IL-11R-E364_V368del does not display any maturation defect. It is present at the cell surface in amounts comparable to IL-11R-WT and fully biologically active in terms of IL-11 classic signaling (Fig. 5D). Further, it is cleaved by the proteases ADAM10 and RHBDL2 and able to perform IL-11

trans-signaling undistinguishable from IL-11R WT. Although the deletion of five amino-acid residues within the stalk region close to the plasma membrane is in close proximity to proteolytic cleavage sites that we have identified previously [12,14], the deletion appears not to directly affect the cleavage events, which can also be explained, at least for the
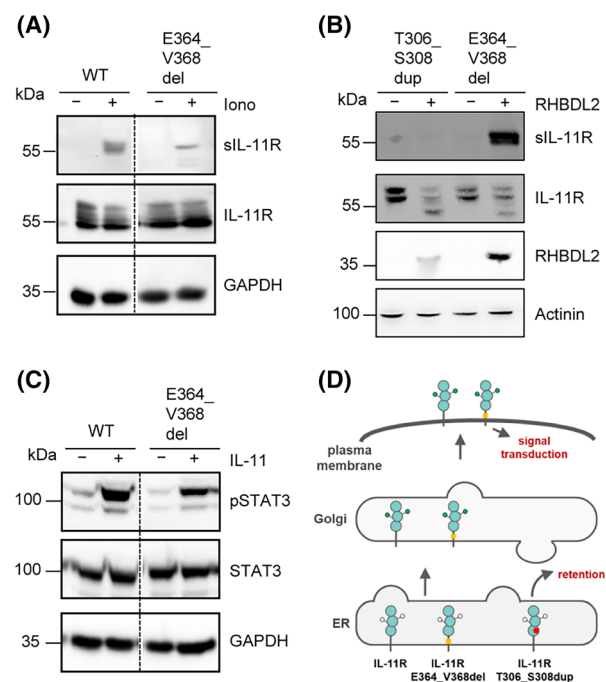
Fig. 5. Proteolysis of IL-11R-E364_V368del results in transsignaling of soluble IL-11R-E364_V368del. (A) HEK293 cells were transiently transfected with expression plasmids encoding IL-11R-WT and IL-11R-E364_V368del variants. Cells were stimulated with 1 μM ionomycin (Iono) or DMSO as control for 1 h at 37 °C. Afterward, cells were lysed and proteins in the supernatant were precipitated. IL-11R in the cell lysate and soluble IL-11R in the supernatant of the two variants was analyzed via western blotting. GAPDH was visualized as loading control. (B) HEK293 cells were transiently co-transfected with expression plasmids encoding either IL-11R-T306_S308dup or IL-11R-E364_V368del in combination with either RHBDL2 or mCherry as a control. Cells were lysed and proteins in the supernatant were precipitated. sIL-11R in the supernatants and IL-11R, RHBDL2 and actinin in the cell lysates were analyzed via western blot. (C) Equal numbers of Ba/F3-gp130 were washed, serum-starved for 120 min and incubated with supernatants of HEK293 cells that were transfected with expression plasmids encoding either IL-11R-WT and RHBDL2 or IL-11R-E364_V368del and RHBDL2 for 15 min. Where indicated, 500 ng·mL^{-1} IL-11 was added to the supernatants prior to stimulation. Cells were lysed and phosphorylation of STAT3 was determined via western blotting. Total STAT3 levels and GAPDH were visualized to ensure equal protein loading. All panels show representative western blots of three independent experiments with similar outcome. Samples unrelated to this manuscript that have been spliced out are indicated by a vertical dashed line. (D) Graphical summary of the findings in this study. Like IL-11R-WT, IL-11R-E364_V368del (yellow) matures properly, is transported to and presented at the plasma membrane and is biologically active. In contrast, IL-11R-T306_S308dup (red) is retained within the cell, not transported to the cell surface and thus not able to perform signal transduction. The two *N*-linked glycans are shown as circles linked to the D2-domain of the IL-11R and are either colored light gray (indicating pre-mature glycans) or green (indicating mature glycans).

metalloprotease ADAM10, with the flexibility of the protease toward the actual cleavage site [56,57]. From these experiments alone, one would argue that a human with the IL-11R-E364_V368del variant should not have a phenotype with features of craniosynostosis. Furthermore, the variant occurred in a single patient in a heterozygous fashion [29], whereas most of the other patients are either homozygous for a mutation or display compound heterozygosity [24]. The fact that the other allele of this patient is unaltered and that the deletion variant is obviously biologically active raises the question of whether the IL-11R mutation is indeed the causative mutation responsible for the craniosynostosis or whether another, so far undetected mutation in a different gene is responsible for the patient's phenotype. Several other genes have been implicated to contribute to craniosynostosis, including *FGFR2*, *TWIST1* and *SKI* [58]. Our data suggest that the craniosynostosis-causing variant in this patient has not been identified so far.

The duplication mutation has been reported in a homozygous state in several individuals with craniosynostosis [29,31], which is in line with our results that it is indeed a loss-of-function mutation. However, the data in this manuscript have been obtained using cell lines overexpressing IL-11R and its variants. It would be desirable to perform similar experiments with cells or cell lines with an endogenous IL-11R expression, which could either be cells from the respective patients or cells which have been genetically modified to express the different IL-11R variants.

Interestingly, the phenotypes of the patients with this mutation differ, even among affected siblings, and it is to date not clear what causes the incomplete penetrance in patients with *IL11RA* mutations. Alterations in skull formation can also be seen in *Ill11ra*$^{-/-}$ mice [29], and also here are only a fraction of the animals affected, whereas others showed no craniosynostosis-like features at all [36]. It appears that another regulatory mechanism is involved, but the nature of this is not known and requires further investigation.

Biochemical characterization of IL-11R variants to determine their biological activity is rather time-consuming, and thus the usage of *in silico* methods to investigate whether a certain mutation leads to loss-of-function of the IL-11R would be desirable. However, our approaches in this direction indicated alterations of the IL-11R structure for both variants analyzed in this study, although our functional data clearly showed that only the variant IL-11R-T306_S308dup is affected, whereas the IL-11R-E364_V368del variant retained its biological activity. This suggests that such an *in silico* analysis

alone at the moment is not sufficient to reliably predict the influence of such changes on the biological function of the IL-11R.

In summary, our study uncovers the molecular basis for two *IL11RA* mutations found in patients with craniosynostosis. Further studies are required to fully understand which mutations of the *IL11RA* are tolerated by the protein and which can be linked to disease.

Materials and methods

Cultivation of cell lines

HEK293 (RRID:CVCL_0045), and HeLa (RRID: CVCL_0030) cells were obtained from ATCC (Manassas, VA, USA). Phoenix-Eco (RRID:CVCL_H717) cells were provided by Stefan Rose-John (Kiel University, Germany). Ba/F3-gp130 cells were obtained from Immunex (Seattle, WA, USA). Original stocks of the cell lines are stored at −150 °C and cells in use were replaced every 10–12 weeks. Morphological and proliferative changes were constantly monitored by all investigators. For the Ba/F3-derived cell lines, the ability to proliferate cytokine-dependently was constantly monitored. All experiments were performed with mycoplasma-free cells; mycoplasma was tested for by PCR quarterly. The authenticity of cell lines was verified through STR profiling. All cells were cultured in DMEM high-glucose culture medium (Pan-biotech, Aidenbach, Germany) supplemented with 10% fetal bovine serum, penicillin (60 mg·L^{-1}), and streptomycin (100 mg·L^{-1}). The medium of Ba/F3-gp130 cells was further supplemented with 10 ng·mL^{-1} Hyper-IL-6. Stably transduced Ba/F3-gp130 cell lines expressing an inactive IL-11R variant were also cultivated with Hyper-IL-6, while Ba/F3-gp130 cell lines expressing a biologically active IL-11R variant were cultured with IL-11 instead. All cells were kept at 37 °C and 5% CO$_2$ in a standard incubator with a water-saturated atmosphere.

Reagents

Ionomycin was purchased from Thermo Fisher Scientific (Waltham, MA, USA). Hyper-IL-6 and IL-11 were produced in house [25,59]. The following antibodies were used: α-HA-tag (C29F4), α-myc-tag (71D10), α-myc-tag (9B11), α-actinin (D6F6), α-GAPDH (14C10), α-pSTAT3 (pTyr705, D3A7), α-STAT3 (124H6), α-GM130 (D6B1), α-rabbit-IgG-HRP-linked and α-mouse-IgG-HRP-linked were obtained from Cell Signaling Technology (Frankfurt, Germany). The fluorescently labeled antibody α-mouse-IgG-Alexa Fluor488 was purchased from Thermo Fisher Scientific, α-rabbit IgG antibody DyLight488 (DI-1488) was purchased from Vector Laboratories (Burlingame, CA, USA) and anti-rabbit-IgG-

IRDye 680RD was obtained from LICOR Biosciences (Lincoln, NE, USA). Wheat Germ Agglutinin (WGA) CF$^®$640R Conjugate was purchased from Biotrend (Cologne, Germany).

Construction of expression plasmids

pcDNA3.1 expression plasmids for myc-tagged hIL-11R have been described previously as well as the expression plasmid encoding the IL-11R variant IL-11R-R296W [36]. The duplication and deletion variants used in this study were generated via splicing by overlapping extension (SOE)-PCR using pcDNA3.1-myc-hIL-11R as template and BoxI/NheI restrictions sites. For stable transduction of Ba/F3-gp130 cells, the open reading frames were sub-cloned into pMOWS plasmids using BoxI/BlpI restriction sites. pcDNA3.1-HA-mRHBDL2 was kindly provided by Dr Matthew Freeman (Sir William Dunn School of Pathology, Oxford, UK) and described previously [60].

Transduction of Ba/F3-gp130 cells

In order to generate Ba/F3-gp130-IL-11R cells stably expressing the variants T306_S308dup and E364_V368del, 5 × 10^5 Phoenix-Eco cells were seeded and the following day transiently transfected with 1 μg of the generated pMOWS plasmids using Turbofect (Thermo Fisher Scientific) according to supplier's instructions. The following day, 1 mL supernatant of the transfected cells was centrifuged at 15 000 *g* at 4 °C for 5 min, before 250 μL of the supernatant with 8 μg·mL^{-1} Polybrene (Sigma-Aldrich, Taufkirchen, Germany) and 1 × 10^5 Ba/F3-gp130 were centrifuged at 500 *g* for 2 h at room temperature. Afterward, cells were cultured in DMEM and cells stably expressing different IL-11R constructs were selected with puromycin (1.5 μg·mL^{-1}) and cultivated with 10 ng·mL^{-1} recombinant Hyper-IL-6 or IL-11.

Analysis of IL-11R proteolysis by RHBDL2

In order to analyze IL-11R proteolysis by RHBDL2, 1 × 10^6 HEK293 cells were seeded and the next day transiently co-transfected with the different IL-11R variants and RHBDL2 or mCherry as control using TurboFect according to suppliers' instructions. The cells were incubated at 37 °C for 48 h, washed with PBS and then incubated in serum-free medium for 5 h. Afterward, supernatants and cells were harvested and prepared for western blot analysis. Supernatants were filtered and then precipitated with 20% trichloroacetic acid, centrifuged at 18 000 *g*, pellets were washed with acetone and centrifuged again at 18 000 *g*. The cells were lysed in 250 μL lysis buffer (50 mM Tris–HCl pH 7.5, 150 mM NaCl, 1% Triton-X-100, complete protease inhibitor cocktail). 30 μg cell lysate were boiled in 2.5× Laemmli buffer and used for western blot analysis.

Analysis of ectodomain shedding by ADAM10

IL-11R cleavage by ADAM10 was analyzed as described previously [14]. In brief, 1×10^6 HEK293 cells were transiently transfected with the different IL-11R variants using TurboFect according to manufacturer's instructions. The next day, the transfected cells were transferred into 6-wells plates. After 24 h, cells were washed with PBS and incubated with 1 µM ionomycin or DMSO as negative control in 1 mL serum-free medium for 1 h at 37 °C. Afterward, supernatants and cells were harvested and prepared for western blot analysis as described above.

Western blotting

Cell lysates and TCA-precipitated proteins were separated under reducing conditions using a SDS/PAGE. For this, 30 µg total protein was loaded onto a 10% SDS gel and run for 2 h at 100 V. Proteins were transferred onto PVDF or nitrocellulose membrane (fluorescence blot) at 100 V for 2 h. Afterward, PVDF membranes were blocked in 5% milk powder whereas nitrocellulose membranes were blocked in 5% BSA in TBS-T for 1 h at room temperature, washed with TBS-T, and incubated with the indicated primary antibody at 4 °C overnight. Membranes were washed with TBS-T and probed with an appropriate secondary antibody conjugated to horseradish peroxidase or a fluorescent-dye (protected from light) for 1 h at room temperature. Afterward, the membrane was washed with TBS-T, and either first incubated with EMD Millipore Immobilon Western Chemiluminescent HRP Substrate (Merck Millipore, Darmstadt, Germany) or immediately detected using the ChemiDoc™ MP Imaging System (BioRad, Feldkirchen, Germany). For the detection of total STAT3 levels, the membrane was stripped for 20 min at room temperature using the Restore Western Blot Stripping Buffer (Thermo Fisher Scientific). The membrane was washed with TBS-T and blocked again for 1 h at room temperature. Afterward, the membrane was washed again with TBS-T and incubated with primary antibody against STAT3 at 4 °C overnight. Secondary antibody incubation and detection were performed as described above.

Immunofluorescence staining and confocal microscopy

Staining of IL-11R variants in transiently transfected HeLa cells has been described previously in detail [40]. In brief, 1×10^6 HeLa cells were seeded on coverslips and transiently transfected 24 h later as described above. 48 h later, cells were fixed for 15 min (4% paraformaldehyde/PBS and 0.02% glutaraldehyde), washed three times and stained with WGA640R (20 µg·mL^{-1} in HBSS) for 10 min at room temperature. Cells were either blocked with 1% BSA/PBS for 10 min or permeabilized with 0.12% Glycine/0.2%

Saponin in PBS for 10 min. After three additional washing steps, cells were blocked with 1% BSA/PBS for 10 min. 0.2% Saponin was added to the blocking solution when the cells were stained intracellularly. After another washing step, cells were stained with α-myc-tag and α-GM130 antibody (1 : 200 in 1% BSA/PBS) for 1 h at room temperature. Afterward, the cells were washed with PBS again and blocked in 1% BSA/PBS before being incubated with secondary AlexaFluor488 and AlexaFluor568 antibodies (1 : 300 in 1% BSA/PBS) for an additional period of 1 h at room temperature. Then, the cells were washed three times with PBS and post fixed with 4% paraformaldehyde/PBS and 0.05% glutaraldehyde. After further washing three times with PBS and once with PBS (pH 8.9), cells were mounted with Vectashield mounting medium containing DAPI (Vector Laboratories, Burlingame, CA, USA) onto microscopy slides.

Slides were visualized using an inverted Confocal Microscope System LeicaSP8 (Leica Mannheim, Germany) equipped with an acousto-optical beam splitter and a Plan Apo 63×/1.4 oil objective and controlled by LASX software (Leica). For the exact setting, please see our previous publication [40].

Flow cytometry

In order to determine IL-11R cell surface levels, transfected HEK293 or stably transduced Ba/F3-gp130-IL-11R cell lines were analyzed via flow cytometry. Cells were washed once in 1% bovine serum albumin/phosphate-buffered saline (BSA/PBS) and stained against IL-11R (α-myc-tag; 1 : 100 in 1% BSA/PBS) for 1 h on ice. Afterward, cells were washed once with 1% BSA/PBS and incubated with a secondary fluorophore-coupled antibody (1 : 100 in 1% BSA/PBS) for 1 h on ice protected from light. Cells were washed three times in 1% BSA/PBS and analyzed using a BD® LSR I Flow Cytometer (BD Bioscience, Franklin Lakes, NJ, USA) controlled by the CELL QUEST PRO software (BD Bioscience). Data analysis was performed using FLOWJO software (BD Bioscience).

Activation of signaling pathways

To analyze pSTAT3 levels in different Ba/F3-gp130-IL-11R cell lines in response to IL-11, cells were washed three times in PBS and 1×10^6 cells were serum-starved for 2 h in DMEM without any supplements. After 2 h, the cells were either stimulated with recombinant IL-11 (10 ng·mL^{-1}), Hyper-IL-6 (10 ng·mL^{-1}) as a positive control or left untreated for 15 min at 37 °C. To analyze pSTAT3 kinetics, the serum-starved cells were stimulated with recombinant IL-11 (10 ng·mL^{-1}) for 0, 15, 30, 60 and 120 min at 37 °C. For the analysis of trans-signaling 300 µL supernatants from RHBDL2 shedding experiments were pre-

incubated with recombinant IL-11 (500 ng·mL^{-1}) for 30 min at 37 °C and serum-starved Ba/F3-gp130 cells were subsequently stimulated with the supernatants for 15 min at 37 °C. Afterward, cells were centrifuged and pellets were resuspended and boiled in 100 μL 2.5× Laemmli buffer. Samples were analyzed via western blot.

Cell viability assay

The response of different Ba/F3-gp130-IL-11R cell lines to IL-11 was measured via the CellTiter Blue Viability Assay (Promega, Fitchburg, WI, USA) following manufacturer's instructions. For this purpose, 5000 cells were seeded in triplicates in a 96-well plate and stimulated with increasing doses of IL-11 or Hyper-IL-6 as a positive control (0–100 ng·mL^{-1}) at 37 °C. After 48 h reaction reagent was added and the fluorescent intensity was measured at 590 nm using FLUOstar Omega (BMG Labtech, Ortenberg, Germany) and normalized to the value received at the starting point.

Deglycosylation of cell lysates

Removal of *N*-glycans with PNGaseF (New England Biolabs, Inc., Ipswich, MA, USA) was performed as described previously [40]. In brief, 30 μg total protein of cell lysates were denatured at 100 °C for 10 min, incubated with 500 units of PNGaseF at 37 °C overnight, boiled in 5× Laemmli buffer and analyzed via western blot.

Structural analysis of the IL-11R mutations

The structure of the IL-11R and the corresponding amino-acid sequence were obtained from the protein database (pdb: 6O4P, [61]). The amino-acid sequence was modified to obtain the IL-11R variants p.T306_S308dup and p.E364_V368del. Structural models were generated by using either COLABFOLD [46] via the Colab notebook (https://colab.research.google.com/github/sokrypton/Colab Fold/blob/main/AlphaFold2.ipynb) or by ROSETTAFOLD [47] via the Robetta server (https://robetta.bakerlab.org/). Obtained structures were superimposed and analyzed to determine the average distance between backbone atoms of superimposed structures. The Matchmaker command ('mm') in UCSF CHIMERAX was used to generate the sequence alignment, superposition, to calculate the root-mean-square deviation (RMSD) of all pruned atom pairs and to visualize the structures [62,63].

Analysis of proteomic datasets

Aiming at the identification of so far unrecognized glycosylated peptides of IL-11R, we used PeptideAtlas [64] to search for proteomic data sets in which IL-11R was identified with high sequence coverage. One of the few samples in which any peptides of IL-11R were observed was from a brain cancer cell line [50]. Using Fragpipe in open search mode [65], we subsequently reanalyzed the public raw data for modified peptides.

Statistical analysis

Statistical analysis was performed using GRAPHPAD PRISM 8 (GraphPad Software, San Diego, CA, USA), and the applied statistical tests were indicated in the respective figure legends.

Conflict of interest

CG has received a research grant from Corvidia Therapeutics (Waltham, MA, USA) and has acted as a consultant for AbbVie and NovoNordisk. All other authors declare no conflict of interest.

Author contributions

BK and A-LH performed the experiments and analyzed the results. RH performed the microscopy experiments together with BK. JL contributed to data analysis and writing of the manuscript. SD and CG performed the computational analyses. HB performed the analysis of the proteomic datasets. FFRB discussed data and analysis and contributed to writing of the manuscript. CG conceived and coordinated the study and wrote the paper. All authors approved the final version of the manuscript.

Peer review

The peer review history for this article is available at https://www.webofscience.com/api/gateway/wos/peer-review/10.1111/febs.17015.

Data availability statement

All data generated or analyzed during this study are included in this published article.

References

1 Garbers C, Hermanns H, Schaper F, Müller-Newen G, Grötzinger J, Rose-John S & Scheller J (2012) Plasticity

and cross-talk of interleukin 6-type cytokines. *Cytokine Growth Factor Rev* **23**, 85–97.

2 Ernst M, Najdovska M, Grail D, Lundgren-May T, Buchert M, Tye H, Matthews V, Armes J, Bhathal P, Hughes N *et al.* (2008) STAT3 and STAT1 mediate IL-11-dependent and inflammation-associated gastric tumorigenesis in gp130 receptor mutant mice. *J Clin Invest* **118**, 1727–1738.

3 Balic JJ, Garbers C, Rose-John S, Yu L & Jenkins BJ (2017) Interleukin-11-driven gastric tumourigenesis is independent of trans-signalling. *Cytokine* **92**, 118–123.

4 Putoczki T, Thiem S, Loving A, Busuttil R, Wilson N, Ziegler P, Nguyen P, Preaudet A, Farid R, Edwards K *et al.* (2013) Interleukin-11 is the dominant IL-6 family cytokine during gastrointestinal tumorigenesis and can be targeted therapeutically. *Cancer Cell* **24**, 257–271.

5 Johnstone CN, Chand A, Putoczki TL & Ernst M (2015) Emerging roles for IL-11 signaling in cancer development and progression: focus on breast cancer. *Cytokine Growth Factor Rev* **26**, 489–498.

6 Winship AL, Van Sinderen M, Donoghue J, Rainczuk K & Dimitriadis E (2016) Targeting interleukin-11 receptor-α impairs human endometrial cancer cell proliferation and invasion in vitro and reduces tumour growth and metastasis in vivo. *Mol Cancer Ther* **15**, 720–730.

7 Schleinkofer K, Dingley A, Tacken I, Federwisch M, Muller-Newen G, Heinrich PC, Vusio P, Jacques Y & Grotzinger J (2001) Identification of the domain in the human interleukin-11 receptor that mediates ligand binding. *J Mol Biol* **306**, 263–274.

8 Nitz R, Lokau J, Aparicio-Siegmund S, Scheller J & Garbers C (2015) Modular organization of Interleukin-6 and Interleukin-11 α-receptors. *Biochimie* **119**, 175–182.

9 Monhasery N, Moll J, Cuman C, Franke M, Lamertz L, Nitz R, Gorg B, Häussinger D, Lokau J, Floss DM *et al.* (2016) Transcytosis of IL-11 and apical redirection of gp130 is mediated by IL-11alpha receptor. *Cell Rep* **16**, 1067–1081.

10 Hilton DJ, Hilton AA, Raicevic A, Rakar S, Harrison-Smith M, Gough NM, Begley CG, Metcalf D, Nicola NA & Willson TA (1994) Cloning of a murine IL-11 receptor alpha-chain; requirement for gp130 for high affinity binding and signal transduction. *EMBO J* **13**, 4765–4775.

11 Yin T, Taga T, Tsang ML, Yasukawa K, Kishimoto T & Yang YC (1993) Involvement of IL-6 signal transducer gp130 in IL-11-mediated signal transduction. *J Immunol* **151**, 2555–2561.

12 Koch L, Kespohl B, Agthe M, Schumertl T, Düsterhöft S, Lemberg MK, Lokau J & Garbers C (2021) Interleukin-11 (IL-11) receptor cleavage by the rhomboid protease RHBDL2 induces IL-11 trans-signaling. *FASEB J* **35**, e21380.

13 Lokau J, Agthe M, Flynn CM & Garbers C (2017) Proteolytic control of Interleukin-11 and Interleukin-6 biology. *Biochim Biophys Acta* **1864**, 2105–2117.

14 Lokau J, Nitz R, Agthe M, Monhasery N, Aparicio-Siegmund S, Schumacher N, Wolf J, Möller-Hackbarth K, Waetzig GH, Grötzinger J *et al.* (2016) Proteolytic cleavage governs interleukin-11 trans-signaling. *Cell Rep* **14**, 1761–1773.

15 Sammel M, Peters F, Lokau J, Scharfenberg F, Werny L, Linder S, Garbers C, Rose-John S & Becker-Pauly C (2019) Differences in shedding of the interleukin-11 receptor by the proteases ADAM9, ADAM10, ADAM17, meprin alpha, meprin beta and MT1-MMP. *Int J Mol Sci* **20**, 3677.

16 Schreiber S, Aden K, Bernardes JP, Conrad C, Tran F, Hoper H, Volk V, Mishra N, Blase JI, Nikolaus S *et al.* (2021) Therapeutic IL-6 trans-signalling inhibition by olamkicept (sgp130Fc) in patients with active inflammatory bowel disease. *Gastroenterology* **160**, 2354–2366.e11.

17 Zhang S, Chen B, Wang B, Chen H, Li Y, Cao Q, Zhong J, Shieh MJ, Ran Z, Tang T *et al.* (2023) Effect of induction therapy with Olamkicept vs placebo on clinical response in patients with active ulcerative colitis: a randomized clinical trial. *JAMA* **329**, 725–734.

18 Lokau J, Garbers Y, Grotzinger J & Garbers C (2021) A single aromatic residue in sgp130Fc/olamkicept allows the discrimination between interleukin-6 and interleukin-11 trans-signaling. *iScience* **24**, 103309.

19 Lokau J, Wandel M & Garbers C (2017) Enhancing Interleukin-6 and Interleukin-11 receptor cleavage. *Int J Biochem Cell Biol* **85**, 6–14.

20 Sun BB, Maranville JC, Peters JE, Stacey D, Staley JR, Blackshaw J, Burgess S, Jiang T, Paige E, Surendran P *et al.* (2018) Genomic atlas of the human plasma proteome. *Nature* **558**, 73–79.

21 Agthe M, Garbers Y, Putoczki T & Garbers C (2017) Interleukin-11 classic but not trans-signaling is essential for fertility in mice. *Placenta* **57**, 13–16.

22 Robb L, Li R, Hartley L, Nandurkar HH, Koentgen F & Begley GC (1998) Infertility in female mice lacking the receptor for interleukin 11 is due to a defective uterine response to implantation. *Nat Med* **4**, 303–308.

23 Bilinski P, Roopenian D & Gossler A (1998) Maternal IL-11Ralpha function is required for normal decidua and fetoplacental development in mice. *Genes Dev* **12**, 2234–2243.

24 Kespohl B, Schumertl T, Bertrand J, Lokau J & Garbers C (2021) The cytokine interleukin-11 crucially links bone formation, remodeling and resorption. *Cytokine Growth Factor Rev* **60**, 18–27.

25 Lokau J, Göttert S, Arnold P, Düsterhöft S, Massa Lopez D, Grötzinger J & Garbers C (2017) The SNP rs4252548 (R112H) which is associated with reduced

human height compromises the stability of IL-11. *Biochim Biophys Acta* **1865**, 496–506.

26 Marouli E, Graff M, Medina-Gomez C, Lo KS, Wood AR, Kjaer TR, Fine RS, Lu Y, Schurmann C, Highland HM *et al.* (2017) Rare and low-frequency coding variants alter human adult height. *Nature* **542**, 186–190.

27 Lanktree MB, Guo Y, Murtaza M, Glessner JT, Bailey SD, Onland-Moret CN, Lettre G, Ongen H, Rajagopalan R, Johnson T *et al.* (2011) Meta-analysis of dense Genecentric association studies reveals common and uncommon variants associated with height. *Am J Hum Genet* **88**, 6–18.

28 Keupp K, Li Y, Vargel I, Hoischen A, Richardson R, Neveling K, Alanay Y, Uz E, Elcioğlu N, Rachwalski M *et al.* (2013) Mutations in the interleukin receptor IL11RA cause autosomal recessive Crouzon-like craniosynostosis. *Mol Genet Genomic Med* **1**, 223–237.

29 Nieminen P, Morgan N, Fenwick A, Parmanen S, Veistinen L, Mikkola M, van der Spek P, Giraud A, Judd L, Arte S *et al.* (2011) Inactivation of IL11 signaling causes craniosynostosis, delayed tooth eruption, and supernumerary teeth. *Am J Hum Genet* **89**, 67–81.

30 Korakavi N, Prokop JW & Seaver LH (2019) Evolution of the phenotype of craniosynostosis with dental anomalies syndrome and report of IL11RA variant population frequencies in a Crouzon-like autosomal recessive syndrome. *Am J Med Genet A* **179**, 668–673.

31 Brischoux-Boucher E, Trimouille A, Baujat G, Goldenberg A, Schaefer E, Guichard B, Hannequin P, Paternoster G, Baer S, Cabrol C *et al.* (2018) IL11RA-related Crouzon-like autosomal recessive craniosynostosis in 10 new patients: resemblances and differences. *Clin Genet* **94**, 373–380.

32 Clarke CM, Fok VT, Gustafson JA, Smyth MD, Timms AE, Frazar CD, Smith JD, Birgfeld CB, Lee A, Ellenbogen RG *et al.* (2018) Single suture craniosynostosis: identification of rare variants in genes associated with syndromic forms. *Am J Med Genet A* **176**, 290–300.

33 Teven CM, Farina EM, Rivas J & Reid RR (2014) Fibroblast growth factor (FGF) signaling in development and skeletal diseases. *Genes Dis* **1**, 199–213.

34 Passos-Bueno M, Sertie Eacute A, Jehee F, Fanganiello R & Yeh E (2008) Genetics of craniosynostosis: genes, syndromes, mutations and genotype-phenotype correlations. *Front Oral Biol* **12**, 107–143.

35 Sims NA, Jenkins BJ, Nakamura A, Quinn JM, Li R, Gillespie MT, Ernst M, Robb L & Martin TJ (2005) Interleukin-11 receptor signaling is required for normal bone remodeling. *J Bone Miner Res* **20**, 1093–1102.

36 Agthe M, Brugge J, Garbers Y, Wandel M, Kespohl B, Arnold P, Flynn CM, Lokau J, Aparicio-Siegmund S, Bretscher C *et al.* (2018) Mutations in craniosynostosis patients cause defective interleukin-11 receptor maturation and drive craniosynostosis-like disease in mice. *Cell Rep* **25**, 10–18.e5.

37 Ahmad I, Lokau J, Kespohl B, Malik NA, Baig SM, Hartig R, Behme D, Schwab R, Altmuller J, Jameel M *et al.* (2023) The interleukin-11 receptor variant p.W307R results in craniosynostosis in humans. *Sci Rep* **13**, 13479.

38 Agthe M, Garbers Y, Grötzinger J & Garbers C (2018) Two N-linked glycans differentially control maturation, trafficking and proteolysis, but not activity of the IL-11 receptor. *Cell Physiol Biochem* **45**, 2071–2085.

39 Karczewski KJ, Francioli LC, Tiao G, Cummings BB, Alfoldi J, Wang Q, Collins RL, Laricchia KM, Ganna A, Birnbaum DP *et al.* (2020) The mutational constraint spectrum quantified from variation in 141,456 humans. *Nature* **581**, 434–443.

40 Kespohl B, Hartig R, Garbers Y, Lokau J & Garbers C (2022) Coding variants of the interleukin-11 receptor with reduced protein maturation show protease-dependent trans-signaling and transduce normal STAT3 signaling. *Genes Dis* **10**, 373–376.

41 Olsen JG & Kragelund BB (2014) Who climbs the tryptophan ladder? On the structure and function of the WSXWS motif in cytokine receptors and thrombospondin repeats. *Cytokine Growth Factor Rev* **25**, 337–341.

42 Dagil R, Knudsen MJ, Olsen JG, O'Shea C, Franzmann M, Goffin V, Teilum K, Breinholt J & Kragelund BB (2012) The WSXWS motif in cytokine receptors is a molecular switch involved in receptor activation: insight from structures of the prolactin receptor. *Structure* **20**, 270–282.

43 Siupka P, Hamming OT, Kang L, Gad HH & Hartmann R (2015) A conserved sugar bridge connected to the WSXWS motif has an important role for transport of IL-21R to the plasma membrane. *Genes Immun* **16**, 405–413.

44 Shcherbakova A, Preller M, Taft MH, Pujols J, Ventura S, Tiemann B, Buettner FF & Bakker H (2019) C-mannosylation supports folding and enhances stability of thrombospondin repeats. *Elife* **8**, e52978.

45 Shcherbakova A, Tiemann B, Buettner FF & Bakker H (2017) Distinct C-mannosylation of netrin receptor thrombospondin type 1 repeats by mammalian DPY19L1 and DPY19L3. *Proc Natl Acad Sci USA* **114**, 2574–2579.

46 Mirdita M, Schutze K, Moriwaki Y, Heo L, Ovchinnikov S & Steinegger M (2022) ColabFold: making protein folding accessible to all. *Nat Methods* **19**, 679–682.

47 Baek M, DiMaio F, Anishchenko I, Dauparas J, Ovchinnikov S, Lee GR, Wang J, Cong Q, Kinch LN, Schaeffer RD et al. (2021) Accurate prediction of protein structures and interactions using a three-track neural network. *Science* **373**, 871–876.

48 Lokau J & Garbers C (2018) The length of the interleukin-11 receptor stalk determines its capacity for classic signaling. *J Biol Chem* **293**, 6398–6409.

49 Mun DG, Bhin J, Kim S, Kim H, Jung JH, Jung Y, Jang YE, Park JM, Kim H, Jung Y et al. (2019) Proteogenomic characterization of human early-onset gastric cancer. *Cancer Cell* **35**, e10.

50 Zhang Y, Zhang K, Bu F, Hao P, Yang H, Liu S & Ren Y (2020) D283 med, a cell line derived from peritoneal metastatic Medulloblastoma: a good choice for missing protein discovery. *J Proteome Res* **19**, 4857–4866.

51 Lokau J, Kespohl B, Kirschke S & Garbers C (2022) The role of proteolysis in interleukin-11 signaling. *Biochim Biophys Acta Mol Cell Res* **1869**, 119135.

52 Lokau J, Agthe M & Garbers C (2016) Generation of soluble Interleukin-11 and Interleukin-6 receptors: a crucial function for proteases during inflammation. *Mediators Inflamm* **2016**, 1785021.

53 Sun Z & Brodsky JL (2019) Protein quality control in the secretory pathway. *J Cell Biol* **218**, 3171–3187.

54 Xu C & Ng DTW (2015) Glycosylation-directed quality control of protein folding. *Nat Rev Mol Cell Biol* **16**, 742–752.

55 Araki K & Nagata K (2011) Protein folding and quality control in the ER. *Cold Spring Harb Perspect Biol* **3**, a007526.

56 Tucher J, Linke D, Koudelka T, Cassidy L, Tredup C, Wichert R, Pietrzik C, Becker-Pauly C & Tholey A (2014) LC-MS based cleavage site profiling of the proteases ADAM10 and ADAM17 using proteome-derived peptide libraries. *J Proteome Res* **13**, 2205–2214.

57 Caescu C, Jeschke G & Turk B (2009) Active-site determinants of substrate recognition by the metalloproteinases TACE and ADAM10. *Biochem J* **424**, 79–88.

58 Topa A, Rohlin A, Andersson MK, Fehr A, Lovmar L, Stenman G & Kolby L (2022) The outcome of targeted NGS screening in patients with syndromic forms of sagittal and pansynostosis – IL11RA is an emerging core-gene for pansynostosis. *Eur J Med Genet* **65**, 104476.

59 Fischer M, Goldschmitt J, Peschel C, Brakenhoff JP, Kallen KJ, Wollmer A, Grötzinger J & Rose-John S (1997) I. A bioactive designer cytokine for human hematopoietic progenitor cell expansion. *Nat Biotechnol* **15**, 142–145.

60 Adrain C, Strisovsky K, Zettl M, Hu L, Lemberg M & Freeman M (2011) Mammalian EGF receptor activation by the rhomboid protease RHBDL2. *EMBO Rep* **12**, 421–427.

61 Metcalfe RD, Aizel K, Zlatic CO, Nguyen PM, Morton CJ, Lio DS, Cheng HC, Dobson RCJ, Parker MW, Gooley PR et al. (2020) The structure of the extracellular domains of human interleukin 11alpha receptor reveals mechanisms of cytokine engagement. *J Biol Chem* **295**, 8285–8301.

62 Pettersen EF, Goddard TD, Huang CC, Couch GS, Greenblatt DM, Meng EC & Ferrin TE (2004) UCSF chimera—a visualization system for exploratory research and analysis. *J Comput Chem* **25**, 1605–1612.

63 Pettersen EF, Goddard TD, Huang CC, Meng EC, Couch GS, Croll TI, Morris JH & Ferrin TE (2021) UCSF ChimeraX: structure visualization for researchers, educators, and developers. *Protein Sci* **30**, 70–82.

64 Deutsch EW (2010) The PeptideAtlas project. *Methods Mol Biol* **604**, 285–296.

65 Geiszler DJ, Polasky DA, Yu F & Nesvizhskii AI (2023) Detecting diagnostic features in MS/MS spectra of post-translationally modified peptides. *Nat Commun* **14**, 4132.